Ultrathin Epitaxial Graphite: 2D Electron Gas Properties and a Route toward Graphene-based Nanoelectronics

Claire Berger,[†] Zhimin Song, Tianbo Li, Xuebin Li, Asmerom Y. Ogbazghi, Rui Feng, Zhenting Dai, Alexei N. Marchenkov, Edward H. Conrad, Phillip N. First, and Walt A. de Heer*

School of Physics, Georgia Institute of Technology, Atlanta, Georgia 30332-0430

Received: October 7, 2004

We have produced ultrathin epitaxial graphite films which show remarkable 2D electron gas (2DEG) behavior. The films, composed of typically three graphene sheets, were grown by thermal decomposition on the (0001) surface of 6H−SiC, and characterized by surface science techniques. The low-temperature conductance spans a range of localization regimes according to the structural state (square resistance 1.5 kΩ to 225 kΩ at 4 K, with positive magnetoconductance). Low-resistance samples show characteristics of weak localization in two dimensions, from which we estimate elastic and inelastic mean free paths. At low field, the Hall resistance is linear up to 4.5 T, which is well-explained by *n*-type carriers of density 10^{12} cm^{-2} per graphene sheet. The most highly ordered sample exhibits Shubnikov−de Haas oscillations that correspond to nonlinearities observed in the Hall resistance, indicating a potential new quantum Hall system. We show that the high-mobility films can be patterned via conventional lithographic techniques, and we demonstrate modulation of the film conductance using a top-gate electrode. These key elements suggest electronic device applications based on nanopatterned epitaxial graphene (NPEG), with the potential for large-scale integration.

1. Introduction

The exceptional electronic transport properties of low-dimensional graphitic structures have been amply demonstrated in carbon nanotubes and nanotube-based transistors. Ballistic transport has been observed up to room temperature,[1−3] and quantum interference effects at cryogenic temperatures.[4−6] Simple nanotube transistors,[7,8] and interconnected logic gates[9] have been demonstrated, which rely on the ability to control the nanotube conductance via an electrostatic gate. The basic transport parameters of these devices are so compelling that nanotubes are considered to be a candidate material system to eventually supplant silicon in many electronic devices.

An under-appreciated fact is that most electronic properties of carbon nanotubes are shared by other low-dimensional graphitic structures. For example, planar nanoscopic graphene ribbons (i.e., ribbons of a single sheet of graphite) have been studied theoretically,[10,11] and they exhibit properties that are similar to nanotubes. Graphene ribbons with either metallic or semiconducting electronic structure are possible, depending on the crystallographic direction of the ribbon axis.[10] Thus, if suitable methods were developed to support and align graphene sheets, it would be possible to combine the advantages of nanotube-like electronic properties with high-resolution planar lithography to achieve large-scale integration of ballistic devices. An essential difference between nanotubes and planar graphene ribbons is the presence of dangling bonds at the edges. Normally these would be hydrogen-terminated, with little influence on the valence electronic properties. However, edge atoms could be passivated with donor or acceptor molecules, thus tuning the electronic properties without affecting the graphitic backbone of the device.

This letter presents recent results[12] that show the two-dimensional nature of electrical transport in ultrathin graphite (multilayered graphene) grown epitaxially on SiC(0001). 6H−SiC is a large band gap (3 eV) semiconductor, which provides an insulating substrate at temperatures below 50 K for the n-type (nitrogen) doping employed here. We use magnetoconductance measurements and the physics of weak localization to determine transport parameters of the graphite 2D electron gas (2DEG), and we show that the character of the magnetotransport/localization spans a wide range of behaviors, depending on the amount of disorder in the film or substrate. Quantum oscillations in the magnetoconductance and in the Hall resistance are found for the most ordered sample. The character of these features suggests that the quantum Hall effect could be observed at lower temperatures, higher fields, or in ultrathin graphite films of only slightly higher mobility. To our knowledge, these are the first transport measurements on oriented and patterned graphite films of only a few monolayers thickness (hence "graphene" films), although related transport experiments have been done on thicker (65−100 graphene layers) free-standing graphite microdisks, which were nanopatterned by focused-ion-beam lithography.[13]

Given the large mean free paths measured in high-quality graphites,[14] the unusual electronic dispersion of graphene, and the fact that the carriers lie near an air-exposed surface, this unique 2DEG system holds great scientific potential. Furthermore, with sufficiently high-quality material, ballistic and coherent devices analogous to nanotube designs[15] would be possible. This goal requires that the epitaxial graphene can survive the processing necessary for creation of submicron ribbons,[10,11] and that the 2DEG can be gated electrostatically. Below we also demonstrate these critical elements for the

* Corresponding author. E-mail: walter.deheer@physics.gatech.edu
[†] Permanent address: CNRS-LEPES, BP166, 38042 Grenoble Cedex, France.

10.1021/jp040650f CCC: $27.50
Published on Web 12/03/2004

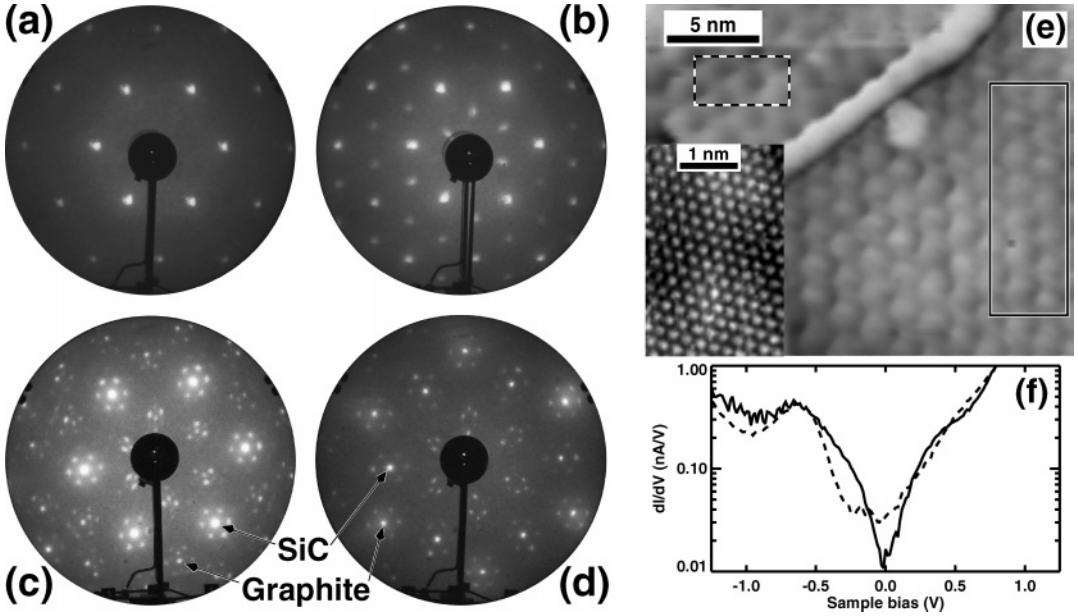

Figure 1. (a−d) LEED patterns from graphite/SiC(0001). The sample was heated several times to successively higher temperatures. (a) 1050 °C for 10 min. Immediately after oxide removal, showing SiC 1 × 1 pattern at 177 eV. AES C:Si ratio 1:2. (b) 1100 °C, 3 min. The $\sqrt{3} \times \sqrt{3}$ reconstruction is seen at 171 eV. AES ratio 1:1.9. (c) 1250 °C, 20 min. 109 eV pattern showing diffracted beams from the $6\sqrt{3} \times 6\sqrt{3}$ unit cell. Examples of first-order SiC and graphite spots are marked. Note the surrounding hexagons of "6 × 6" spots. AES C:Si ratio 2:1 (∼1 ML graphite). (d) 1400 °C, 8 min. 98 eV LEED pattern. AES ratio 7.5:1 (∼2.5 ML graphite). (e) STM image of a surface region of the sample described in Figure 1d. Inset: Atomically resolved region (different sample, similar preparation). (f): d*I*/d*V* spectra (log scale) acquired from the regions marked with corresponding line types in the image at top. The solid line is an average of 396 spectra at different positions, the dashed line an average of 105. With a few "glitchy" exceptions, individual spectra in each region showed negligible variation from the average d*I*/d*V* shown.

realization of electronic devices based on nanopatterned epitaxial graphene (NPEG).

2. Results and Discussion

Ultrathin epitaxial graphite films were produced on the Si-terminated (0001) face of single-crystal 6H−SiC by thermal desorption of Si.[16−19] After surface preparation by oxidation[20] or H_2 etching,[21] samples were heated by electron bombardment in ultrahigh vacuum (UHV; base pressure 1×10^{-10} Torr) to ∼1000 °C in order to remove the oxide (some samples were oxidized/deoxidized several times to improve the surface quality). Scanning force microscopy images showed that the best initial surface quality was obtained with H_2 etching (sample A). After verifying by Auger electron spectroscopy (AES) that the oxide was removed, samples were heated to temperatures ranging from 1250 °C to 1450 °C for 1−20 min. Under these conditions, thin graphite layers are formed,[16−18] with the layer thickness determined predominantly by the temperature. Multilayered graphene film thicknesses were estimated by modeling the ratio of measured intensities in the Si 92-eV and C 271-eV Auger peaks (3 keV incident energy).[22−24]

Figures 1a−d show low energy electron diffraction patterns (LEED) at different stages during the growth of a 2.5-monolayer (ML) graphite film grown in situ. Figure 1e displays an STM image from the sample obtained after stage d. The image reveals a distinct 6 × 6 corrugation of the overlayer[25] and a raised region along a step on the surface. This modulation has been previously attributed to variations of the interlayer interaction arising from Moiré coincidences between the graphite and SiC lattices within a fundamental $6\sqrt{3} \times 6\sqrt{3}$ surface unit cell.[16,25−27] LEED confirms that the graphene sheets register epitaxially with the underlying SiC, as shown in Figures 1c and 1d. The mean height difference between terraces (0.25 nm), indicates that the step in Figure 1e is a bilayer step in the SiC substrate. Terrace sizes (corresponding to a single 6 × 6 domain) are found by STM to be up to several hundred nanometers in extent. Preliminary high-resolution LEED studies indicate that the graphene layers are strained in-plane by 0.3−0.5%, with a mean structural coherence length of greater than 20 nm.

Also shown in Figure 1f are derivative tunneling spectra (d*I*/d*V* vs *V*) acquired within the respective boxed regions of the image. The d*I*/d*V* spectrum obtained from the lower terrace (solid line) is similar to that of a zero-gap semiconductor, as found typically for bulk graphite. On the upper terrace, the 6 × 6 domain images somewhat differently, and the d*I*/d*V* spectrum (dashed line) displays a region of constant, finite conductance around the Fermi energy (zero bias). Spectral shapes are very uniform within each 6 × 6 domain. The d*I*/d*V* curves show that the electronic properties of the film are not entirely homogeneous. This may relate to differing lateral registry (i.e., not orientational) of the graphite on the SiC substrate, or electron confinement within 6 × 6 domains. d*I*/d*V* spectra acquired over the buckled region at the step edge are nearly identical to those found on the upper terrace, suggesting that the graphite layer remains continuous over the step.

DC and low-frequency AC conductance measurements were made for temperatures $T = 0.3-50$ K and for magnetic fields H from 0−8 T on graphite films with thicknesses of typically 3 graphene sheets (see Table 1). For Hall-effect measurements, samples were defined using standard optical lithography (photoresist coating, plasma etching, photoresist removal via solvents). Four contacts were painted with silver paste directly on the surface or on evaporated Pd−Au pads on mm-sized samples. For samples B, C, and E, the voltage probe distance d_V is 2 mm. For the Hall bar samples A and D $d_V = 600$ and 300 μm respectively (see photo inset, Figure 2a). Reported values below are the square conductance G.

The 2D nature of electrical transport in the film is vividly demonstrated in Figure 2a by the large anisotropy in the magnetoconductance [MC = $G(H)$]: For sample E, for H

TABLE 1: Sample Properties[a]

Sample	C:Si	Thickness	R_{4K}	Mobility
A	10	3 ML	1.5 $k\Omega$	1100 cm^2/Vs
B	∞	>5	2.2	
C	9	3	22	
D	10	3	33	15
E	9	3	225	
F	7	2.5		

[a] Ratio of intensities in the C(271 eV) and Si(92 eV) AES peaks, calculated thickness in graphene monolayers, square resistance at 4 K, and mobility (where measured).

perpendicular to the graphene plane the differential magnetoconductance (dMC = dG/dH) is large and positive (3.0 μS/T at 4 K), whereas there is essentially no response when H lies in the plane (in-plane MC was measured with H transverse to the current direction). This anisotropy is found in all of our samples and indicates that the motion of charge carriers is confined to the graphene planes. The observed positive dMC is in contrast to bulk graphite,[28] which shows negative dMC for well-ordered single-crystals, and also a large anisotropy. However, carbon foils fabricated from exfoliated graphite[29] and partially graphitic carbons[30] have positive dMCs initially, which become negative at large fields. This behavior is a consequence of disorder-induced localization in the sample.

Figure 2a shows systematic changes in the perpendicular MC for samples of successively larger zero-field conductance (i.e., decreasing disorder). For sample C the initial 4 K slope is larger, at 30 μS/T, and the MC attains an approximately temperature-independent maximum of 185 μS at $H \approx 3.5$ T. Sample A shows even more structure. Following a large initial dMC (180 μS/T at 4 K), the MC maximizes near 1.5 T, then decreases, followed by a series of (Shubnikov−de Haas) oscillations. A temperature-independent "fixed point" at $G = 680\ \mu S$ and $H = 7.4$ T is also observed.

As a function of temperature, the conductance increases proportional to ln T at low T, as shown in Figure 2b for samples A−C. This is quite characteristic of a 2D electron gas in the weak localization regime.[31,32] The least conductive samples (D and E; $G < e^2/h = 38.8\ \mu$S) deviate slightly from the ln T dependence, which is indicative of a transition to strong localization (see for instance ref 33).

In a 2D system, carriers will localize at low temperature due to constructive quantum interference of time-reversed paths for carriers scattered elastically from static disorder.[31] The interference is reduced (conductance increased) by breaking time-reversal symmetry through the application of a magnetic field, or by increasing temperature. These coherent effects are manifest when the elastic mean free path l_e is smaller than the inelastic mean free path $l_i(T)$. For $k_F l_e \gg 1$ (k_F is the Fermi wave vector), the system is in the weak localization regime. Strong localization occurs for smaller $k_F l_e$.[33,34]

Shown in the center panel inset of Figure 2a are the perpendicular MC of sample B for five different temperatures (circles) and fits to the data according to 2D weak localization theory (lines).[32] The entire family of MC curves is fit by a single temperature-dependent parameter, $l_i(T)$. Note that for transport in two dimensions, the mean free paths are obtained from the modeling without knowledge of either the Fermi velocity or the carrier effective mass. For sample B, we find $l_e = 15$ nm and $l_i = 100$ nm at $T = 4$ K. Weak localization effects are observed over a much smaller range of magnetic field for sample A, but a similar estimate gives $l_e = 20-30$ nm and a much larger inelastic mean free path $l_i(4\text{ K}) \sim 300$ nm. From the carrier density $n = 10^{12}$ cm^{-2} per graphene sheet (see below), we find for sample A $k_F l_e \sim 5$, in agreement with the weak localization regime.

In two cases we have observed a reversal of the dMC. At the maximum MC for sample C (Figure 2a), the conductance per graphene sheet (Table 1) is 1.5 e^2/h, i.e., comparable to the conductance quantum. This behavior, and the large change in MC of this sample (320%) are reminiscent of disordered 2DEGs, which have been explained in terms of a transition from an Anderson insulator to a quantum Hall liquid.[35] The second case is that of sample A, which underwent an improved substrate preparation. For this sample, we also observe an initial maximum in the MC, but at much lower field (1.5 T). Apparently, weak localization dominates the MC behavior of sample A in the low-field region, but the longer scattering paths are dephased by a smaller magnetic field. The subsequent appearance of Shubnikov−de Haas oscillations indicates quantization of the electron energy spectrum and wave function coherence on a scale comparable to the cyclotron radius (~30 nm at 5 T), which is consistent with the elastic scattering lengths estimated above. The significance of the quasi-temperature-independent fixed point at 680 μS and a field of 7.4 T is not yet fully understood. Note that $1/H$ at the crossing point is equal to the mobility obtained from Hall measurements (see below). This correspondence would be an expected consequence of electron−electron interactions under weak localization,[33,36] but the observed quantum oscillations show that at high fields the system is beyond this regime.

The Hall resistance R_{xy} was measured for samples D and A in the Hall bar configuration (photo inset, Figure 2a) at a bias current of 100 nA. For sample D at 4 K, R_{xy} versus H is linear from 0 to 8 T, with the slope corresponding to a density $n = 10^{13}$ cm^{-2} n-type charge carriers, and a mobility of 15 cm^2/Vs. The Hall voltage is also linear up to 4.5 T in sample A, from which we determine $n = 3.6 \times 10^{12}$ cm^{-2} (n-type), and an enhanced mobility of 1100 cm^2/Vs. The observation of a linear Hall effect is particularly remarkable, since single-crystal graphite samples display a substantial quadratic component at small fields,[29,37−39] due to three subbands (one electron, two hole). Apparently, our samples cannot be thus described. The carrier densities found here are comparable to those of other 2DEG systems, although the density per graphene sheet (~10^{12} cm^{-2}) is higher than that found in high-quality graphites.[28,38,39] It remains to be determined what effect substrate doping has on the carrier density and mobility in the graphite film.

For the case of sample A, a carrier density can be obtained from the period (in $1/H$) of the Shubnikov−de Haas oscillations. Assuming a circular 2D Fermi surface, we estimate $n = 10^{12}$ cm^{-2} ($k_F = 2.5 \times 10^6$ cm^{-1}). The carrier density determined by the Hall effect is very nearly a factor 3 larger, which is the number of graphene layers measured via AES. Clearly, the simplest explanation would be that each graphene sheet supports a 2D electron gas which remains confined within the sheet. This would be consistent with the large anisotropy in conductivity for bulk graphite.[28] The temperature dependences of samples A−C also support this interpretation: dG/d (ln T) falls between 2.5 $e^2/\pi h$ and 3.5 $e^2/\pi h$, about a factor 3 larger than the predicted weak localization contribution to the conductance, of the order of $e^2/\pi h$ ln T.[32]

Above 4.5 T in sample A, we observe nonlinearities in R_{xy} vs H, as shown in Figure 2a (lower-panel inset) for $T = 4$ K. These coincide with the Shubnikov−de Haas oscillations in the magnetoconductance, showing that they have the same origin: either broadened quantum Hall plateaus or bulk magnetoquantum oscillations in a metallic system. If the Hall conductance

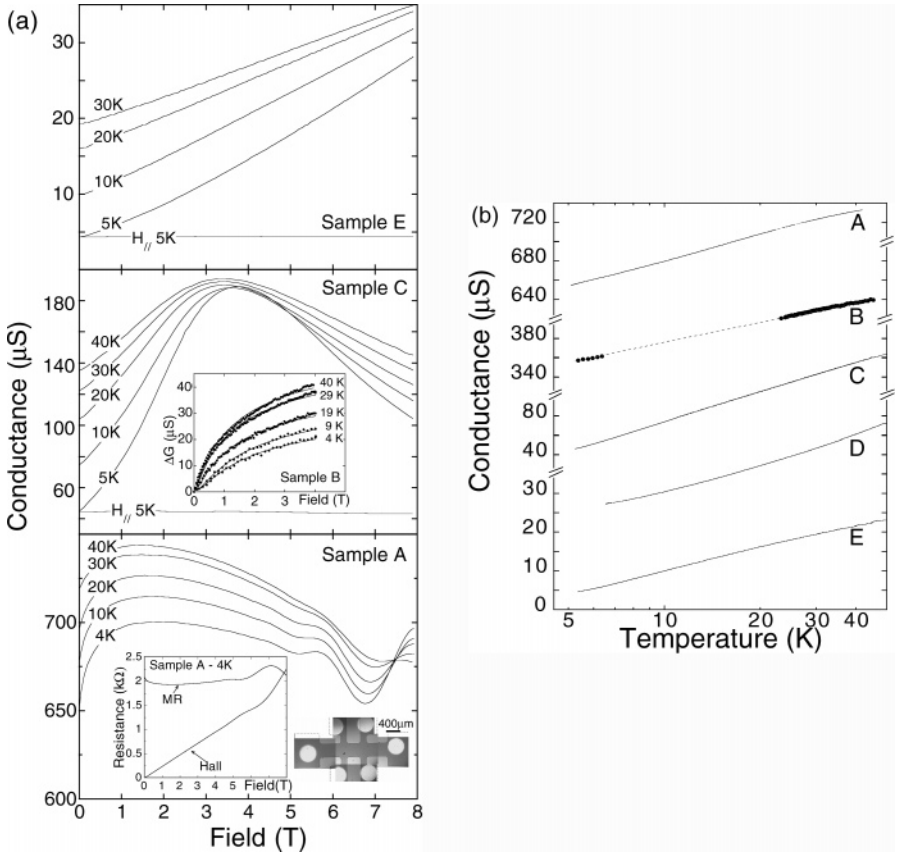

Figure 2. (a) Magnetoconductance $G(H)$ for samples E, C, and A in perpendicular field for temperatures as indicated. Also shown for samples E and C, the in-plane magnetoconductance at 5 K. Note the strong anisotropy between the perpendicular and in-plane field configuration. In sample C, the conductance goes through a maximum at about the same value of field and conductance for all T. In sample A Shubnikov−de Haas oscillations develop at high magnetic field. Center-panel inset: $G(H) - G(H = 0)$ for sample B. Solid curve are fits to the weak localization theory with no spin−orbit, yielding elastic scattering length $l_e \approx 15$ nm and inelastic scattering length l_i (4 K) ≈ 100 nm. Lower-panel inset: Hall resistance $R_{xy} = V_{xy}/i$ and magnetoresistance R_{xx} as a function of magnetic field at 4 K for sample A. Below 4.5 T, R_{xy} is remarkably linear, indicative of n-type carriers. At high magnetic field, the oscillations coincide with the oscillations in the magnetoresistance. (b) Square conductance as a function of temperature for samples of various conductance (samples A, B, C, D, and E from top to bottom). Note that the conductance scale is × 4 for samples D and E, compared to the scale for sample A−C. Samples A, B, and C show a ln T form in this decade of temperature, characteristic of 2D weak localization.

at the location of the local maximum (≈5.5 T) is normalized with respect to the number of sheets, one obtains a conductance $\sim 4\ e^2/h$, which suggests a quantum Hall effect (see also predictions in ref 40). Experiments at lower temperatures and higher fields will be necessary to verify this conjecture.

At 0.3 K, we also observe a pronounced zero-bias anomaly in the highly resistive sample D. The conductance is found to increase by about a factor 10 as the bias voltage is increased from 0 to 25 mV.[41] For weak electron−electron interactions it can be understood in terms of enhanced scattering of carriers near the Fermi energy: the wavelengths of these carriers are commensurate with the Friedel oscillations surrounding impurities, thus they scatter strongly. The coherence is lost at higher bias (higher kinetic energies). Zero-bias anomalies have also been observed in carbon nanotubes.[42−44]

It should be noted that the samples are remarkably stable over time. For instance, measurements in Figures 2a and 2b were made four months earlier than those in the lower-panel inset of Figure 2a, with no particular storage precautions. The features observed are essentially the same, except for a slight decrease in conductance and carrier density. The results presented above for sample A also show that the multisheet epitaxial graphene film survives conventional lithographic processing extraordinarily well.

Finally, as a preliminary demonstration of the device potential of this new 2DEG system, a large-area gated graphite channel

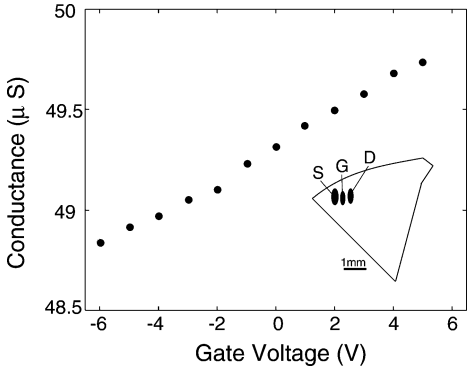

Figure 3. Conductance as a function of gate voltage for sample F at 4 K. Inset, sketch of the sample showing the contacts and top-gate geometry (S, D, G = source, drain, gate). The top gate is only partially effective due to the open geometry. Nevertheless, a 2% change in conductance is observed.

field effect transistor (FET) structure was assembled. A schematic of the "device" is shown in Figure 3, as well as the measured source−drain resistance as a function of gate voltage. The top-gate structure consisted of a conductive coating on a 100-nm-thick insulating aluminum oxide layer. The gate covered only a portion of the graphite film between the source and drain electrodes, leaving large ungated leakage paths (see inset, Figure 3). Consequently, the resistance modulation is rather small (2%),

but these results show clearly that multisheet epitaxial graphene films can be gated, in distinct contrast to thicker samples.[45] Thus we anticipate that FET-type devices will be possible, particularly when the channel electronic structure is controlled by patterning the graphite into a narrow strip.[10,13,46]

3. Conclusion

The experimental results presented here demonstrate the rich scientific promise of ultrathin epitaxial graphite ("graphene") films. Several points should be appreciated. First, the production method allows graphitic films to be grown epitaxially, as evidenced by LEED and STM measurements. From Auger spectroscopy we further conclude that the layers involve only a few graphene sheets. Remarkably, the films are electrically continuous over several mm. Magnetoconductance measurements clearly reveal 2D electron gas properties, including large anisotropy, high mobility, and 2D localization, in samples patterned by conventional lithography. Quantum oscillations observed in both the magnetoconductance and the Hall resistance indicate a potential new quantum Hall system. Finally, control of the 2D electron gas carrier density via electrostatic gating was also demonstrated.

Considered with prior research in graphitic systems, these results provide ample evidence that the graphite/SiC system could provide a platform for a new breed of seamlessly integrated ballistic carrier devices based on nanopatterned epitaxial graphene. Such an architecture could have many advantages for nanoelectronics, including potentially coherent devices, energy efficiency, and facile integration with molecular devices.

Acknowledgment. This work was funded by Intel Research and by the Department of Energy (DE-FG02-02ER45956). Support from Georgia Tech, CNRS-France, and the NSF (ECS-0404084), is also gratefully acknowledged. We thank Drs. Thierry Klein, Jacques Marcus, and Frédéric Gay, CNRS-LEPES, Grenoble-France, for their generosity in allowing us to use their cryostats, and Dr. P. G. Neudeck, NASA Glenn Research Center, for supplying the sample used in Figure 1. We are especially grateful to Dr. Thierry Grenet for providing invaluable assistance in obtaining the data in Figure 3.

Note Added in Proof. While this paper was in press, the electric field effect on the transport of thin graphite sheets was confirmed by K. S. Novoselov et al., *Science* **2004**, *306*, 666.

References and Notes

(1) Frank, S.; Poncharal, P.; Wang, Z.; Heer, W. D. *Science* **1998**, *280*, 1744.

(2) Poncharal, P.; Berger, C.; Yi, Y.; Wang, Z.; de Heer, W. *J. Phys. Chem. B* **2002**, *106*, 12104.

(3) Liang, W.; Bockrath, M.; Bozovic, D.; Hafner, J.; Tinkham, M.; Park, H. *Nature* **2001**, *411*, 665.

(4) Tans, S.; Devoret, M.; Dai, H.; Thess, A.; Smalley, R.; Georliga, L.; Dekker, C. *Nature* **1997**, *386*, 474.

(5) Bachtold, A.; Strunk, C.; Salvetat, J.-P.; Bonard, J.-M.; Forro, L.; Nussbaumer, T.; Schönenberger, C. *Nature* **1999**, *397*, 673.

(6) Schönenberger, C.; Bachtold, A.; Strunk, C.; Salvetat, J.; Forro, L. *Appl. Phys. A* **1999**, *A69*, 283.

(7) Tans, S.; Verschueren, R.; Dekker, C. *Nature* **1998**, *393*, 49.

(8) Martel, R.; Schmidt, T.; Shea, H.; Hertel, T.; Avouris, P. *Appl. Phys. Lett.* **1998**, *73*, 2447.

(9) Bachtold, A.; Hadley, P.; Nakanishi, T.; Dekker, C. *Science* **2001**, *294*, 1317.

(10) Wakabayashi, K. *Phys. Rev. B* **2001**, *64*, 125428-1.

(11) Nakada, K.; Fujita, M.; Dresselhaus, G.; Dresselhaus, M. *Phys. Rev. B* **1996**, *54*, 17954.

(12) Berger, C.; Song, Z.; Li, T.; First, P. N.; Bellissard, J.; de Heer, W. A. *Bull. Am. Phys. Soc.* **2004**, *49*, A17.8.

(13) Dujardin, E.; Thio, T.; Lezec, H.; Ebbesen, T. *Appl. Phys. Lett.* **2001**, *79*, 2474.

(14) Kaburagi, Y.; Yoshida, A.; Hishiyama, Y. *J. Mater. Res.* **1996**, *11*, 769.

(15) Javey, A.; Guo, J.; Wang, Q.; Lundstrom, M.; Dai, H. *Nature* **2003**, *424*, 654.

(16) Bommel, A. V.; Crombeen, J.; Tooren, A. V. *Surf. Sci.* **1975**, *48*, 463.

(17) Charrier, A.; Coati, A.; Argunova, T.; Thibaudau, F.; Garreau, Y.; Pinchaux, R.; Forbeaux, I.; Debever, J.-M.; Sauvage-Simkin, M.; Themlin, J.-M. *J. Appl. Phys.* **2002**, *92*, 2479.

(18) Forbeaux, I.; Themlin, J.-M.; Debever, J.-M. *Phys. Rev. B* **1998**, *58*, 16396.

(19) Samples for transport measurements were obtained from Cree, Inc., Durham, NC (research grade, *n*-doped, 0.05 Ω-cm). Figures 1 and 2 show LEED and STM data from a sample with a 1-μm CVD layer grown at the NASA Glenn Research Center. The CVD sample was initially much smoother than the as-received Cree sample. However, after oxidation/graphitization cycles, samples were found via LEED and STM to be similar, although the CVD sample was still of higher overall surface quality.

(20) Cho, M.-H.; Shin, J.; Roh, Y.; Lyo, I.-W.; Jeong, K.; Whang, C.; Lee, J.; Yoo, J.; Lee, N.; Fujihara, K.; Moon, D. W. *J. Vac. Sci. Technol. A* **2003**, *21*, 1004.

(21) Ramachandran, V.; Brady, M. F.; Smith, A. R.; Feenstra, R. M.; Greve, D. W. *J. Elec. Mater.* **1998**, *27*, 308.

(22) Li, T.; Ogbazghi, A. Y.; First, P. N., to be published.

(23) Tanuma, S.; Powell, C. J.; Penn, D. R. *Surf. Interface Anal.* **1991**, *17*, 911.

(24) Tanuma, S.; Powell, C. J.; Penn, D. R. *Surf. Interface Anal.* **1991**, *17*, 927.

(25) Tsai, M.-H.; Chang, C.; Dow, J.; Tsong, I. *Phys. Rev. B* **1992**, *45*, 1327.

(26) Starke, U.; Franke, M.; Bernhardt, J.; Schardt, J.; Reuter, K.; Heinz, K. *Mater. Sci. Forum* **1998**, *264*−*268*, 321.

(27) Owman, F.; Martensson, P. *Surf. Sci.* **1996**, *369*, 126.

(28) Soule, D. E.; McClure, J. W.; Smith, L. B. *Phys. Rev.* **1964**, *134*, A453.

(29) Schaijk, R. V.; Visser, A. D.; Ionov, S.; Kulbachinskii, V.; Kytin, V. *Phys. Rev. B* **1998**, *57*, 8900.

(30) Bayot, V.; Piraux, L.; Michenaud, J.-P.; Issi, J.-P.; Lelaurain, M.; Moore, A. *Phys. Rev. B* **1990**, *41*, 11770.

(31) Abrahams, E.; Anderson, P.; Licciardello, D.; Ramakrishnan, T. *Phys. Rev. Lett.* **1979**, *42*, 673.

(32) Bergmann, G. *Phys. Rep.* **1984**, *107*, 1.

(33) Minkov, G.; Rut, O.; Germanenko, A.; Sherstobitov, A.; Zvonkov, B.; Uskova, E.; Birukov, A. *Pys. Rev. B* **2002**, *65*, 235322-1.

(34) The strong localization regime is not discussed in detail here, but we note that for samples D and E, measurements in the range 0.3−2 K show $\ln(G) \sim T^{-1/3}$, a form that is consistent with theories of strong localization in 2D.[47]

(35) Jiang, H.; Johnson, C.; Wang, K.; Hannahs, S. *Phys. Rev. Lett.* **1993**, *71*, 1439.

(36) Altshuler, B.; Aronov, A. Electron−electron interaction in disordered conductors. In *Electron−electron interactions in disordered systems*; Efros, A. L.; Pollak, M., Eds.; Elsevier Science Publishers: Amsterdam, 1985.

(37) Berlincourt, T. G.; Steele, M. C. *Phys. Rev.* **1955**, *98*, 956.

(38) Du, X.; Tsai, S.-W.; Maslov, D. L.; Hebard, A. F. *arXiv:* cond-mat/0404725, **2004**.

(39) Tokumoto, T.; Jobiliong, E.; Choi, E.; Oshima, Y.; Brooks, J. *Solid State Comm.* **2004**, *129*, 599.

(40) Zheng, Y.; Ando, T. *Phys. Rev. B* **2002**, *65*, 245420-1.

(41) Samples were carefully mounted with the connecting wires thermally connected by stycast epoxy to the cooled copper plate. This mounting provided more than sufficient thermal coupling to ensure that the maximum power into the sample (10 nW) did not cause significant heating.

(42) Bockrath, M.; Cobden, D.; Lu, J.; Rinzler, A.; Smalley, R.; Balents, L.; McEuen, P. *Nature* **1999**, *397*, 598.

(43) Tarkiainen, R.; Ahlskog, M.; Penttila, J.; Roschier, L.; Hakonen, P.; Paalanen, M.; Sonin, E. *Phys. Rev. B* **2001**, *64*, 195412-1.

(44) Yi, W.; Lu, L.; Hu, H.; Pan, Z.; Xie, S. *Phys. Rev. Lett.* **2003**, *91*, 076801-1.

(45) Kempa, H.; Esquinazi, E. *arXiv: cond-mat/0304105* **2003**.

(46) Cancado, L.; Pimenta, M.; Neves, B.; Medeiros-Ribeiro, G.; Enoki, T.; Kobayashi, Y.; Takai, K.; Fukui, K.; Dresselhaus, M.; Saito, R.; Jorio, A. *Phys. Rev. Lett.* **2004**, *93*, 047403.

(47) Mott, N. F. *Conduction in Non-Crystalline Materials;* Oxford University Press: New York, 1987.